NANO LETTERS

2007
Vol. 7, No. 5
1396−1400

Electromigrated Nanoscale Gaps for Surface-Enhanced Raman Spectroscopy

Daniel R. Ward,[†] Nathaniel K. Grady,[‡] Carly S. Levin,[§] Naomi J. Halas,[§,||] Yanpeng Wu,[‡] Peter Nordlander,[†,||] and Douglas Natelson*[,†,||]

Department of Physics and Astronomy, Applied Physics Graduate Program, Department of Chemistry, Department of Electrical and Computer Engineering, and the Rice Quantum Institute, Rice University, 6100 Main Street, Houston, Texas 77005

Received March 15, 2007; Revised Manuscript Received April 2, 2007

ABSTRACT

Single-molecule detection with chemical specificity is a powerful and much desired tool for biology, chemistry, physics, and sensing technologies. Surface-enhanced spectroscopies enable single-molecule studies, yet reliable substrates of adequate sensitivity are in short supply. We present a simple, scaleable substrate for surface-enhanced Raman spectroscopy (SERS) incorporating nanometer-scale electromigrated gaps between extended electrodes. Molecules in the nanogap active regions exhibit hallmarks of very high Raman sensitivity, including blinking and spectral diffusion. Electrodynamic simulations show plasmonic focusing, giving electromagnetic enhancements approaching those needed for single-molecule SERS.

Multifunctional sensors with single-molecule sensitivity are greatly desired for a variety of sensing applications, from biochemical analysis to explosives detection. Chemical and electromagnetic interactions between molecules and metal substrates are used in surface-enhanced spectroscopies[1] to approach single- molecule sensitivity. Electromagnetic enhancement in nanostructured conductors results when incident light excites local electronic modes, producing large electric fields in a nanoscale region, known as a "hot spot", that greatly exceed the strength of the incident field. Hot spots can lead to particularly large enhancements of Raman scattering because the Raman scattering rate is proportional to $|\mathbf{E}(\omega)|^2|\mathbf{E}(\omega')|^2$ at the location of the molecule, where $\mathbf{E}(\omega)$ is the electric field component at the frequency of the incident radiation, and $\mathbf{E}(\omega')$ is the component at the scattered frequency.

It has been an ongoing challenge to design and fabricate a substrate for systematic SERS at the single-molecule level. Single-molecule SERS sensitivity was first clearly demonstrated using random aggregates of colloidal nanoparticles.[2−5] Numerous other metal substrate configurations have been used for SERS, including chemically engineered nanoparticles,[6−8] nanostructures defined by bottom-up patterning,[9,10] and those made by traditional lithographic approaches.[11] In the most sensitive substrate geometries, incident light excites adjacent subwavelength nanoparticles or nanostructures, resulting in large field enhancements within the interparticle gap.[12,13] Fractal aggregates of nanoparticles[14] can further increase field enhancements by focusing plasmon energy from larger length scales down to particular nanometer-scale hotspots.[15] However, precise and reproducible formation of such assemblies in predetermined locations has been extremely challenging. An alternative approach is tip-enhanced Raman spectroscopy (TERS), in which the incident light excites an interelectrode plasmon resonance localized between a sharp, metal scanned probe tip and an underlying metal substrate. Recent progress has been made in single-molecule TERS detection.[16−18] A similar approach was recently attempted using a mechanical break junction.[19] While useful for surface imaging, TERS requires feedback to control the tip−surface gap and is not scalable or readily integrated with other sensing modalities.

We demonstrate a scaleable and highly reliable method for producing planar extended electrodes with nanoscale spacings that exhibit very large SERS signals, with each electrode pair having one well-defined hot spot. Confocal scanning Raman microscopy demonstrates the localization of the enhanced Raman emission. The SERS response is consistent with a very small number of molecules in the hotspot, showing blinking and spectral diffusion of Raman lines. Sensitivity is sufficiently high that SERS from physisorbed atmospheric contaminants may be detected after minutes of exposure to ambient conditions. The Raman enhancement for *para*-mercaptoaniline (*p*MA) is estimated from experimental data to exceed 10^8. Finite-difference time-domain (FDTD) modeling of realistic structures reveals a

* Corresponding author. E-mail: natelson@rice.edu.
[†] Department of Physics and Astronomy.
[‡] Applied Physics Graduate Program.
[§] Department of Chemistry.
[||] Department of Electrical and Computer Engineering.

10.1021/nl070625w CCC: $37.00
Published on Web 04/13/2007

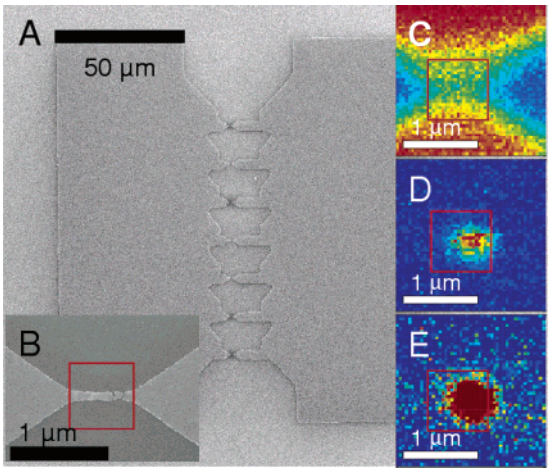

Figure 1. (A) Full multibowtie structure, with seven nanoconstrictions. (B) Close-up of an individual constriction after electromigration. Note that the resulting nanoscale gap (<~5 nm at closest separation, as inferred from closer images) is toward the right edge of the indicated red square. (C) Map of Si Raman peak (integrated from 500 to 550 cm^{-1}) in device from (B), with red corresponding to high total counts. The attenuation of the Si Raman line by the Au electrodes is clear. (D) Map of *p*MA SERS signal for this device based on one carbon ring mode (integrated from 1050 to 1110 cm^{-1}). (E) Map of integrated low-energy background (50−300 cm^{-1}) for this device.

rich collection of interelectrode plasmon modes that can readily lead to SERS enhancements as large as 5×10^{10} over a broad range of illumination wavelengths. These structures hold the promise of integration of single-molecule SERS with electronic transport measurements, as well as other near-field optical devices.

Our structures are fabricated on a Si wafer topped by 200 nm of thermal oxide. Electron beam lithography is used to pattern "multibowtie" structures as shown in Figure 1A. The multibowties consist of two larger pads connected by multiple constrictions, as shown. The constriction widths are 80−100 nm, readily within the reach of modern photolithography. After evaporation of 1 nm Ti and 15 nm Au, followed by liftoff in acetone, the electrode sets are cleaned of organic residue by exposure to O_2 plasma for 1 min. The multibowties are placed in a vacuum probe station, and electromigration[20] is used to form nanometer-scale gaps in the constrictions in parallel, as shown in Figure 1B. Electromigration is a nonthermal process whereby momentum transfer from current-carrying electrons is transferred to the lattice, rearranging the atomic positions. Electromigration has been studied thoroughly[21−24] as a means of producing electrodes for studies of single-molecule conduction. We have performed manual and automated electromigration at room temperature, with identical results. The number of parallel constrictions in a single multibowtie is limited by the output current capacity of our electromigration voltage source. A postmigration resistance of ~10 kΩ for the structure in Figure 1A appears optimal.

Postmigration high-resolution scanning electron microscopy (SEM) shows interelectrode gaps ranging from too small to resolve to several nanometers. There are no detectable nanoparticles in the gap region or along the electrode edges. On the basis of electromigration of 283 multibowties (1981 individual constrictions), 77% of multibowties have final resistances less than 100 kΩ and 43% have final resistances less than 25 kΩ. We believe that this yield, already high, can be improved significantly with better process control, particularly of the lithography and liftoff.

The optical properties of the resulting nanogaps are characterized using a WITec CRM 200 scanning confocal Raman microscope in reflection mode, with normal illumination from a 785 nm diode laser. Using a 100× objective, the resulting diffraction-limited spot is measured to be Gaussian with a full width at half-maximum of 575 nm. Figure 1C shows a spatial map of the integrated emission from the 520 cm^{-1} Raman line of the Si substrate. The Au electrodes are clearly resolved. Polarization of the incident radiation is horizontal in this figure. Rayleigh-scattered light from these structures shows significant changes upon polarization rotation, while SERS response is approximately *independent* of polarization.

Freshly cleaned nanogaps show no Stokes-shifted Raman emission out to 3000 cm^{-1}. However, in 65% of clean nanogaps examined, a broad continuum background (see Supporting Information) is seen, decaying roughly linearly in wavenumber out to 1000 cm^{-1} before falling below detectability. This background is spatially localized to a diffraction-limited region around the interelectrode gap and is entirely absent in unmigrated junctions. The origin of this continuum, similar to that seen in other strongly enhancing SERS substrates,[5] is likely inelastic electronic effects in the gold electrodes.[25] In samples coated with molecules, this background correlates strongly with visibility of SERS. No junctions without this background displayed SERS signals. Like the SERS signal, this background is approximately polarization independent. Temporal fluctuations of this background in clean junctions are minimal, strongly implying that fluctuations of the electrode geometry are not responsible for SERS blinking.

The SERS enhancement of the junctions has been tested using various molecules. The bulk of testing utilized *p*MA, which self-assembles onto the Au electrodes via standard thiol chemistry. Particular modes of interest are carbon ring modes at 1077 and 1590 cm^{-1}. Figure 1D shows a map of the Raman emission from the 1077 cm^{-1} line on the same junction as Figure 1B,C after self-assembly of *p*MA. This emission is strongly localized to the position of the nanogap. No Raman signal is detectable either on the metal films or at the edges of the metal electrodes. Figure 1E shows the spatial localization of the continuum background mentioned above.

Figure 2 shows a more detailed examination of the SERS response of the gap region of a typical junction after self-assembly of *p*MA. Figure 2A,B are time series of the SERS response, with known *p*MA modes indicated. The modes visible are similar to those seen in other SERS measurements of *p*MA on lithographically fabricated Au structures.[11] Each spectrum was acquired with 1 s integration time, with the objective positioned over the center of the nanogap hotspot. Temporal fluctuations of both the Raman intensity ("blink-

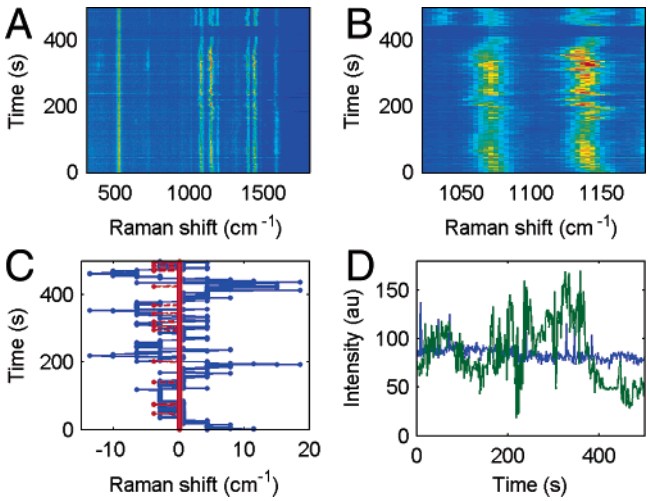

Figure 2. (A) Waterfall plot (1 s integration steps) of SERS spectrum at a single nanogap that had been soaked in 1 mM *p*MA in ethanol. Identified *p*MA peaks include the ring modes at 1077 cm^{-1} and 1590 cm^{-1}, as well as an 1145 cm^{-1} δCH mode with b_2 symmetry, an 1190 cm^{-1} mode identified as δCH of a_1 symmetry, a mode near 1380 cm^{-1} identified as δCH + νCC of b_2 symmetry, and a mode near 1425 cm^{-1} identified as νCC + δCH of b_2 symmetry. Mode assignments are based on ref 27. (B) Close-up of (A) to show correlated wandering and blinking of 1077 cm^{-1} and 1145 cm^{-1} modes. (C) Comparison of 1145 cm^{-1} mode position (blue) with the Si Raman peak (red), which shows no such wandering. The jitter in the Si peak position is 1 pixel in the detector. (D) Comparison of 1145 cm^{-1} peak height (green, found by a Gaussian fit to the peak) fluctuations with those of the Si peak (blue).

ing") and Raman shift (spectral diffusion), generally regarded as hallmarks of few- or single-molecule SERS sensitivity,[26] are readily apparent. Figure 2C shows a comparison of the wandering of the 1077 cm^{-1} *p*MA line with that of the 520 cm^{-1} Raman line of the underlying Si substrate over the same time interval. This demonstrates that the spectral diffusion is due to changes in the molecular environment rather than a variation in spectrometer response. Figure 2D shows the variation in the peak amplitudes over that same time interval.

This blinking and spectral diffusion are seen *routinely* in these junctions. We have observed such Raman response from several molecules, including self-assembled films of *p*MA, *para*-mercaptobenzoic acid (*p*MBA), a Co-containing transition metal complex,[28] and spin-coated poly(3-hexylthiophene) (P3HT). These molecules all have distinct Raman responses and show blinking and wandering in the junction hotspots.

Another indicator of very large enhancement factors in these structures is sensitivity to exogenous, physisorbed contamination. Carbon contamination has been discussed[29–31] in the context of both SERS and TERS. This substrate is sensitive enough to examine such contaminants (see Supporting Information). While clean junctions with no deliberately attached molecules initially show only the continuum background, gap-localized SERS signatures in the sp^2 carbon region between 1000 and 1600 cm^{-1} are readily detected after exposure to ambient lab conditions for tens of minutes. Nanojunctions that have been coated with a self-assembled monolayer (SAM) (for example, *p*MA) do *not* show this

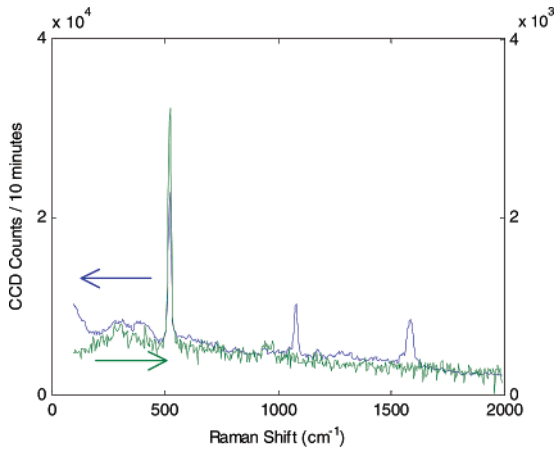

Figure 3. Blue curve (left scale): *p*MA SERS spectrum at hotspot center of one nanojunction densely covered by *p*MA, integrated for 10 min at incident power of 700 μW. Green curve (right scale): integrated signal under same conditions on middle of Au pad on the same nanojunction. The feature near 960 cm^{-1} is from the Si substrate. No Raman features are detectable on either the Au pads or their edges under these conditions.

carbon signature, even after hours of ambient exposure. Presumably this has to do with the extremely localized field enhancement in these structures, with the SAM sterically preventing physisorbed contaminants from entering the region of enhanced near field.

Recently arrived contaminant SERS signatures abruptly disappear within tens of seconds at high incident powers (1.8 mW), presumably due to desorption. SERS from covalently bound molecules is considerably more robust, degrading slowly at high powers and persisting indefinitely for incident powers below 700 μW. SEM examination of the nanogaps shows no optically induced damage after exposure to intensities that would significantly degrade nanoparticles.[32] The large extended pads likely aid in the thermal sinking of the nanogap region to the substrate.

Estimating enhancement factors rigorously is notoriously difficult, particularly when the hotspot size is not known. Although SERS enhancement volume measurements are possible using molecular rulers,[33] this is not feasible with such small nanogaps. Junctions made directly on Raman-active substrates (Si with no oxide; GaAs) show no clearly detectable enhancement of substrate modes in the gap region, suggesting that the electromagnetic enhancement is strongly confined to the thickness of the metal film electrodes. Figure 3 shows a comparison between a typical *p*MA SERS spectrum acquired on a junction with a 600 s integration time at 700 μW incident power and a spectrum acquired over one of that device's Au pads for the same settings. The pad spectrum shows no detectable *p*MA features and is dark current limited.

We use FDTD calculations to understand the strong SERS response in these structures and roughly estimate enhancement factors. It is important to note that the finite grid size (2 nm) required for practical computation times restricts the quantitative accuracy of these calculations. However, the main results regarding spatial mode structure (allowing assessment of the localization of the hotspot) and energy

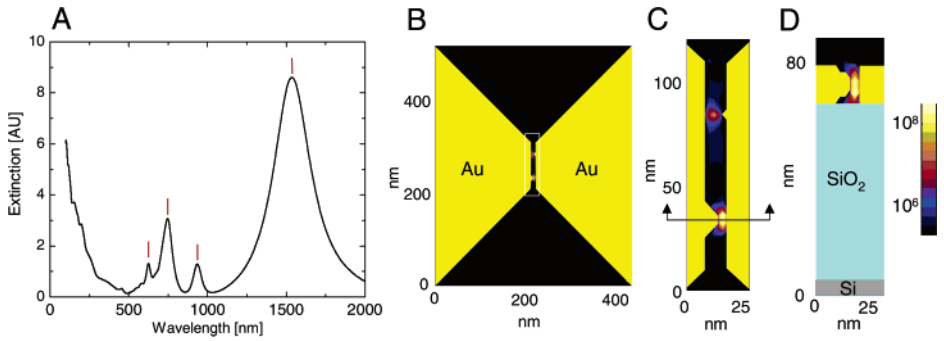

Figure 4. (A) FDTD-calculated extinction spectrum from the model electrode configuration shown in (B). (B) Mock-up electrode tips capped with nanoscale hemispherical asperities, with $|\mathbf{E}|^4$ plotted for the 937 nm resonance of (A). Constriction transverse width at narrowest point is 100 nm. Gap size without asperities is 8 nm. Asperity on left (right) electrode has radius of 6 nm (4 nm). Au film thickness is 15 nm, SiO_2 underlayer thickness is 50 nm. Radiation is normally incident, with polarization oriented horizontally. Grid size for FDTD calculation is 2 nm. (C) Close-up of central region of (B), showing extremely localized enhancement at asperities. (D) Cross section indicated in (C), showing that enhancement in this configuration does not penetrate significantly into the substrate. Predicted maximum electromagnetic Raman enhancement in this mode exceeds 10^8.

dependence are robust to these concerns, and the calculated electric field enhancement is an *underestimate*.[34] Figure 4 shows a calculated extinction spectrum and map of $|\mathbf{E}|^4$ in the vicinity of the junction. Calculational details and additional plots are presented in the Supporting Information. These calculations predict that there should be large SERS enhancements across a broad bandwidth of exciting wavelengths because of the complicated mode structure possible in the interelectrode gap. Nanometer-scale asperities from the electromigration process break the interelectrode symmetry of the structure. The result is that optical excitations at a variety of polarizations can excite many interelectrode modes besides the simple dipolar plasmon commonly considered. For extended electrodes, a continuous band of plasmon resonances coupling to wavelengths from 500 to 1000 nm is expected.[35] This broken symmetry also leads to much less dependence of the calculated enhancement on polarization direction, as seen experimentally. The calculations confirm that the electromagnetic enhancement is confined in the normal direction to the film thickness. Laterally, the field enhancement is confined to a region comparable to the radius of curvature of the asperity. For gaps and asperities in the range of 2 nm, purely electromagnetic enhancements can exceed 10^{11}, approaching that sufficient for single-molecule sensitivity.

Using the data from the device in Figure 3, we estimate the total enhancement in that device. To be conservative, we assume a hotspot effective radius of 2.5 nm with dense packing of *p*MA, giving $N \approx 100$ molecules. Blinking and wandering suggest that the true N value is much closer to one. The integrated Raman signal over a Gaussian fit to the 1077 cm^{-1} Raman line is 2.0 counts/s/molecule when the incident power is 700 μW. For our apparatus, the count rate from imaging a bulk crystal at the same equivalent power (see Supporting Information) is 4.2×10^{-9} counts/s/molecule, so that we estimate a total enhancement of at least 5×10^8.

We have demonstrated a SERS substrate capable of extremely high sensitivity for trace chemical detection. Unlike previous substrates, these nanojunctions may be mass fabricated in controlled positions with high yield using a combination of standard lithography and electromigration. The resulting hotspot geometry is predicted to allow large SERS enhancements over a broad band of illuminating wavelengths. Other nonlinear optical effects should be observable in these structures as well. The extended electrode geometry and underlying gate electrode are ideal for integration with other sensing modalities such as electronic transport. Tuning molecule/electrode charge transfer via the gate electrode may also enable the direct examination of the fundamental nature of chemical enhancement in SERS.

Acknowledgment. D.W. acknowledges support from the NSF-funded Integrative Graduate Research and Educational Training (IGERT) program in Nanophotonics. N.H., P.N., and D.N. acknowledge support from Robert A. Welch Foundation grants C-1220, C-1222, and C-1636, respectively. D.N. also acknowledges the National Science Foundation, the David and Lucile Packard Foundation, the Sloan Foundation, and the Research Corporation. C.S.L. was supported by a training fellowship from the Keck Center Nanobiology Training Program of the Gulf Coast Consortia, NIH 1 T90 DK070121-01. Y.P. and N.K.G. are supported by U.S. Army Research Office grant W911NF-04-1-0203.

Supporting Information Available: Detailed examination of continuum background and adsorption of exogenous contaminants; extended discussion of FDTD calculations; more detailed discussion of SERS enhancement calculation. This material is available free of charge via the Internet at http://pubs.acs.org.

References

(1) Moskovits, M. *Rev. Mod. Phys.* **1985**, *57*, 783−826.
(2) Kneipp, K.; Wang, Y.; Kneipp, H.; Perelman, L. T.; Itzkan, I.; Dasari, R. R.; Feld, M. S. *Phys. Rev. Lett.* **1997**, *78*, 1667−1670.
(3) Nie, S.; Emory, S. R. *Science* **1997**, *275*, 1102−1106.
(4) Xu, H.; Bjerneld, E. J.; Käll, M.; Börjesson, L. *Phys. Rev. Lett.* **1999**, *83*, 4357−4360.
(5) Michaels, A. M.; Jiang, J.; Brus, L. *J. Phys. Chem. B* **2000**, *104*, 11965−11971.

(6) Jackson, J. B.; Halas, N. J. *Proc. Natl. Acad. Sci. U.S.A.* **2004**, *101*, 17930−17935.
(7) Wang, H.; Levin, C. S.; Halas, N. J. *J. Am. Chem. Soc.* **2005**, *127*, 14992−14993.
(8) Oldenburg, S. J.; Westcott, S. L.; Averitt, R. D.; Halas, N. J. *J. Chem. Phys.* **1999**, *111*, 4729−4735.
(9) Haynes, C. L.; Van Duyne, R. P. *J. Phys. Chem. B* **2001**, *105*, 5599−5611.
(10) Qin, L.; Zou, S.; Xue, C.; Atkinson, A.; Schatz, G. C.; Mirkin, C. A. *Proc. Natl. Acad. Sci. U.S.A.* **2006**, *103*, 13300−13303.
(11) Fromm, D. P.; Sundaramurthy, A.; Kinkhabwala, A.; Schuck, P. J.; Kino, G. S.; Moerner, W. E. *J. Chem. Phys.* **2006**, *124*, 061101.
(12) Hallock, A. J.; Redmond, P. L.; Brus, L. E. *Proc. Natl. Acad. Sci. U.S.A.* **2005**, *102*, 1280−1284.
(13) Nordlander, P.; Oubre, C.; Prodan, E.; Li, K.; Stockman, M. I. *Nano Lett.* **2004**, *4*, 899−903.
(14) Wang, Z.; Pan, S.; Krauss, T. D.; Du, H.; Rothberg, L. J. *Proc. Natl. Acad. Sci. U.S.A.* **2003**, *100*, 8638−8643.
(15) Li, K.; Stockman, M. I.; Bergman, D. J. *Phys. Rev. Lett.* **2003**, *91*, 227402.
(16) Domke, K. F.; Zhang, D.; Pettinger, B. *J. Am. Chem. Soc.* **2006**, *128*, 14721−14727.
(17) Neascu, C. C.; Dreyer, J.; Behr, N.; Raschke, M. B. *Phys. Rev. B* **2006**, *73*, 193406.
(18) Zhang, W.; Yeo, B. S.; Schmid, T.; Zenobi, R. *J. Phys. Chem. C* **2007**, *111*, 1733−1738.
(19) Tian, J.-H.; Liu, B.; Li, X.; Yang, Z.-L.; Ren, B.; Wu, S.-T.; Tao, N.; Tian, Z.-Q. *J. Am. Chem. Soc.* **2006**, *128*, 14748−14749.
(20) Park, H.; Lim, A. K. L.; Alivisatos, A. P.; Park, J.; McEuen, P. L. *Appl. Phys. Lett.* **1999**, *75*, 301−303.
(21) Strachan, D. R.; Smith, D. E.; Johnston, D. E.; Park, T. H.; Therien, M. J.; Bonnell, D. A.; Johnson, A. T. *Appl. Phys. Lett.* **2005**, *86*, 043109.
(22) Trouwborst, M. L.; van der Molen, S. J.; van Wees, B. J. *J. Appl. Phys.* **2006**, *99*, 114316.
(23) Strachan, D. R.; Smith, D. E.; Fischbein, M. D.; Johnston, D. E.; Guiton, B. S.; Drndic, M.; Bonnell, D. A.; Johnson, A. T. *Nano Lett.* **2006**, *6*, 441−444.
(24) Taychatanapat, T.; Bolotin, K. I.; Kuemmeth, F.; Ralph, D. C. *Nano Lett.* **2007**, *7*, 652−656.
(25) Beversluis, M. R.; Bouhelier, A.; Novotny, L. *Phys. Rev. B* **2003**, *68*, 115433.
(26) Wang, Z.; Rothberg, L. J. *J. Phys. Chem. B* **2005**, *109*, 3387−3391.
(27) Osawa, M.; Matsuda, N.; Yoshii, K.; Uchida, I. *J. Phys. Chem.* **1994**, *98*, 12702−12707.
(28) Ciszek, J. W.; Keane, Z. K.; Cheng, L.; Stewart, M. P.; Yu, L. H.; Natelson, D.; Tour, J. M. *J. Am. Chem. Soc.* **2006**, *128*, 3179−3189.
(29) Kudelski, A.; Pettinger, B. *Chem. Phys. Lett.* **2000**, *321*, 356−362.
(30) Otto, A. *J. Raman Spectrosc.* **2002**, *33*, 593−598.
(31) Richards, D.; Milner, R. G.; Huang, F.; Festy, F. *J. Raman Spectrosc.* **2003**, *34*, 663−667.
(32) Schuck, P. J.; Fromm, D. P.; Sundaramurthy, A.; Kino, G. S.; Moerner, W. E. *Phys. Rev. Lett.* **2005**, *94*, 017402.
(33) Lal, S.; Grady, N. K.; Goodrich, G. P.; Halas, N. J. *Nano Lett.* **2006**, *6*, 2338−2343.
(34) Oubre, C.; Nordlander, P. *J. Phys. Chem. B* **2005**, *109*, 10042−10051.
(35) Nordlander, P.; Le, F. *Appl. Phys. B* **2006**, *84*, 35−41.

NL070625W